Millimeter Wave Picocellular System Evaluation for Urban Deployments

Mustafa Riza Akdeniz, *Student Member, IEEE*, Yuanpeng Liu, *Student Member, IEEE*, Sundeep Rangan, *Senior Member, IEEE*, Elza Erkip, *Fellow, IEEE*

***Abstract*—With the severe spectrum shortage in conventional cellular bands, millimeter wave (mmW) frequencies between 30 and 300 GHz have been attracting growing attention as a possible candidate for next-generation micro- and picocellular wireless networks. The mmW bands offer orders of magnitude greater spectrum than current cellular allocations and enable very high-dimensional antenna arrays for further gains via beamforming and spatial multiplexing. However, the propagation of mmW signals in outdoor non line-of-sight (NLOS) links remains challenging and the feasibility of wide-area mmW cellular networks is far from clear. This paper uses recent real-world measurements at 28 GHz in New York City to provide a realistic assessment of mmW picocellular networks in a dense urban deployment. It is found that, even under conservative propagation assumptions, mmW systems with cell radii of 100m can offer an order of magnitude increase in capacity over current state-of-the-art 4G cellular networks with similar cell density. However, it is also shown that such mmW networks may operate in a largely power-limited regime where the full spatial and bandwidth degrees of freedom are not fully utilized. This power-limited regime contrasts significantly with current bandwidth-limited cellular systems, requiring alternate technologies for mmW systems that may unlock further gains that mmW frequency bands offer.**

***Index Terms*—millimeter wave radio, 3GPP LTE, cellular systems, wireless propagation, 28 GHz, urban deployments.**

I. Introduction

With the popularity of today's smartphones and tablets, demand for cellular wireless data is projected to grow at a staggering rate necessitating new technologies that can offer orders of magnitude increases in network capacity [1], [2]. To address this challenge, there has been growing interest in cellular systems based in the so-called *millimeter-wave* (mmW) bands, between 30 and 300 GHz, where the available bandwidths are much wider than today's cellular networks [3]–[6]. Indeed, the available spectrum at these frequencies can be easily 200 times greater than all cellular allocations today that are currently largely constrained to prime RF real estate under 3 GHz [4]. Moreover, the very small wavelengths of mmW signals combined with advances in low-power CMOS RF circuits enable large numbers of miniaturized antennas to be placed in small dimensions. These multiple antenna systems can be used to form very high gain, electrically steerable arrays, fabricated at the base station, in the skin of a cellphone, or even within a chip [5], [7]–[13].

This material is based upon work supported by the National Science Foundation under Grants No. 1116589 and 1237821.

M. Akdeniz (email:makden01@students.poly.edu), Y. Liu (email:yliu20@students.poly.edu), S. Rangan (email: srangan@poly.edu) E. Erkip (email: elza.edu) are with the Polytechnic Institute of New York University, Brooklyn, NY.

However, while mmW communication has been successfully used for backhaul and short-range indoor communication [14]–[16], its applicability to longer range wide-area networks is challenging and the feasibility of such systems remains an open question. Most importantly, the propagation of mmW signals is much less favorable than signals in conventional microwave bands. Friis' transmission law [17] states that free-space path loss grows with the square of the frequency. This fact alone implies that increasing transmission frequencies of current cellular systems around 2 GHz to the 30–300 GHz range would result in an immediate 20 to 30 dB increase in the path loss. Moreover, mmW signals are extremely susceptible to shadowing. For example, materials such as brick can attenuate signals by as much as 80 dB [4], [18]–[20] and the human body itself can result in a 20 to 35 dB loss [21].

To assess the feasibility of the mmW cellular networks, Rappaport *et. al.* [22]–[25] have recently performed an extensive set of measurements to characterize NLOS propagation of mmW signals in New York City at 28 GHz. While millimeter wave signals have been extensively characterized in indoor environments [26]–[31], models for mmW propagation in outdoor settings such as [32]–[34] have not yet been verified experimentally. The models [22]–[25] thus provide a unique opportunity to systematically evaluate mmW small cell networks in a dense urban environment based on real experimental data. In this paper, we combine the empirical propagation models derived in [22]–[25] with an industry-standard cellular 3GPP evaluation framework [35], [36] to estimate both the capacity and cell edge throughput under various deployment and device options.

We focus on urban outdoor environments since the high user density, small cell radii (typically 100 to 200m) and lower mobility makes urban settings a natural candidate for initial deployments of mmW picocellular networks. However, at the same time, the urban topology is a particularly challenging setting for mmW signals due to the lack of LOS connectivity, severe shadowing as well limitations on the height and placement of cells.

Our key finding is that mmW picocellular networks offer a possible order of magnitude increase in capacity over current cellular systems. Specifically, our simulations show that a hypothetical 1 GHz TDD mmW picocellular network offers more than 15x capacity over an LTE 20+20 MHz FDD MIMO (2x2 downlink, 2x4 uplink) LTE system (see Table III).

Moreover, it should be emphasized that our study, if anything, is conservative. As we will describe in Section II, the measurements in [22]–[25] on which our evaluation is based,

focussed on NLOS propagation where LOS data points were largely excluded from the measurements. In contrast, earlier studies [3], [6], [32], [37] which used either analytic models or commercial ray tracing software, generally assumed that propagation was dominated by either LOS links or links with a few strong specular reflections. Naturally, these studies get even higher capacity estimates than shown here. It is possible that, with proper cell placement, a significant fraction of mobiles may in reality experience stronger LOS links as predicted in these earlier analytic studies. The goal of this paper, however, is to provide a conservative "lower bound" on the capacity estimates that can be validated with experimental data and show that, even in complete absence of LOS connectivity, large gains of mmW systems are possible.

Nevertheless, under these conservative assumptions, our simulations also indicate that mmW systems are potentially power-limited and thus operate in a fundamentally different regime than current cellular networks in dense interference-limited deployments. As a consequence, the enormous bandwidth and spatial degrees of freedom afforded by the mmW spectrum may not be fully utilized in the current cellular deployment model. As part of future research, we suggest alternate technologies such as multihop relaying that may be able to unlock these degrees of freedom and increase the gains of mmW systems even further.

II. Channel Models

A. Measurement Methodology

As discussed in the Introduction, the path loss and multi-input multi-output (MIMO) spatial models in this study are based on recent 28 GHz measurements in New York City [22], [24]. To mimic microcellular type networks, transmitters were placed on rooftops two to five stories high and measurements were then made at a number of street level locations up to 200m from the transmitters (see Fig. 1). To characterize both the bulk path loss and spatial structure of the channels, measurements were performed with highly directional horn antennas (10 degree beamwidths, 24.5 dBi gain each side). At each transmitter (TX) - receiver (RX) location pair, the angles of the TX and RX antennas were swept across a range of values to detect discrete clusters of paths. Empirical statistical models were then fit to this data to describe a variety of channel characteristics including the number of clusters, path loss per cluster, cluster angular spread, etc.

In this paper, we use the non-line of sight (NLOS) models in [22], [24] where the bulk of data was collected. However, it must be emphasized that the predominance of NLOS points seen in [22], [24] may be a feature of the particular measurement methodology – not necessarily an inherent feature of urban deployments. Indeed, it is possible that with different cell placement (e.g. below rooftops or street poles), more street-level locations could have been exposed to LOS paths or paths with strong specular reflections as assumed in earlier analytic studies mentioned in the Introduction. Therefore, the results in this paper should be considered as a conservative or "worst-case" analysis. Actual capacity gains of mmW systems may be even larger than what our results suggest.

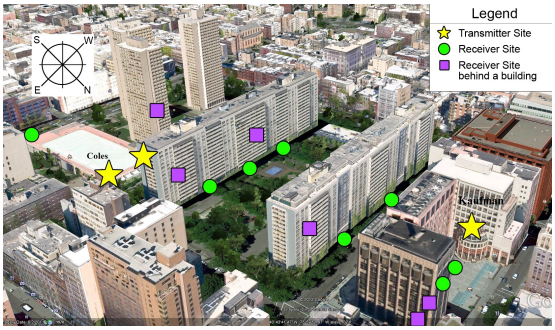

Fig. 1: Image from [22] showing typical measurement locations in NYC at 28 GHz for which the path loss models in this paper are derived.

B. Large-Scale Path Loss Model

The large-scale parameters for the NLOS models are summarized in Table I. The parameters are based both on the original papers [22], [24], as well as extended models that will be presented in a submitted paper [25]. As described in Table I, the channel between each TX-RX pair is assumed to consist of $K = 3$ clusters, with the path loss of each cluster of the form $\alpha + 10\beta \log_{10}(d)$ with independent lognormal shadowing, where the values for α and β taken from [25]. The measurements in [24] reported minimal horizonal angular spread at the TX or vertical angular spread at either the TX and RX. Hence, the evaluation model here assumes that the BS central horizontal angle of departure (AoD) and all vertical angles are the same for all clusters. However, the horizontal angle-of-arrivals (AoA) of the $K = 3$ clusters at the UE are independent and distributed uniformly in $[0, 2\pi]$. Following [24], the horizontal angles of the subpaths within each cluster are then generated uniformly with in an interval of $[-\delta, \delta]$ around the cluster central angle.

The parameters in Table I – namely, the number of clusters K, and the per cluster path losses, central angles and angular spread – together represent the *large-scale* parameters that are assumed to change slowly since they depend only on the macro-scattering environment. In the simulation, an independent set of large-scale parameters are generated for each link and are assumed to be constant. Each link, however, will experience a time-varying MIMO channel matrix $\mathbf{H}$ whose variations are due to the small-scale fading. We follow a standard model [35] to describe the small scale variations which is reviewed in Appendix A.

C. Comparison to Other Models

For comparison, Fig. 2 plots the path loss model used in this paper along with several previous models. The model used in this paper, as described above, is shown on the curve labeled "empirical NYC". The curve shows the effective average *omni-directional* path loss found by non-coherent combining of the energy across all K clusters, but not applying any beamforming gain. As discussed in Appendix B, this path loss is given by

$$PL_{\text{omni}} = -10 \log_{10} \left[\sum_{k=1}^{K} 10^{-0.1 PL_k} \right], \qquad (1)$$

TABLE I: Large-scale path loss and beamforming parameters

Parameter	Value
Number of clusters K	3
Per cluster shadowing S_k	*Lognormal* $(0, \sigma)$, $\sigma = 8.36$ dB
Per cluster path loss PL_k	$PL_k = 75.85 + 37.3 \log_{10}(d) + S_k$, d in meters
BS and UE vertical central cluster AoD and AoA, $\bar{\phi}^T$ and $\bar{\phi}^R$	Single value common to all BS and UEs and clusters within each BS and UE. No vertical angular separation is assumed.
BS horizontal central cluster AoD, $\bar{\theta}_k^T$	*Uniform*$[0, 2\pi]$, common to all clusters from the BS.
UE horizontal central cluster AoA, $\bar{\theta}_k^R$	*Uniform*$[0, 2\pi]$, independent for all clusters from the UE.
BS and UE cluster vertical angular spread	0
BS and UE cluster horizonal angular spread, δ_k^R, δ_k^T	*Exponential*(λ) mod $360°$, $\lambda^{-1} = 7.8°$. Common to all clusters from BS, but independent between clusters to UE. Subpaths generated uniformly with angles $[-\delta, \delta]$ around horizontal AoA and AoD.
Antenna array	$\lambda/2$ uniform 2D 8×8 antenna array at both base station and UE. (64 antennas each side).

where PL_k is the per cluster path loss (including shadowing). It is immediately seen that this path loss is significantly higher than several other models:

- *Free-space:* The theoretical free space path loss is given by Friis' Law [17]. We see that, at $d = 100$ m (our target cell radius), the free-space path loss is more than 43 dB less than the model we have assumed here.
- *PLF1:* This is the first of two models used in Samsung study [3] which is simply free space propagation plus 20 dB. Even with the 20 dB correction factor, this model is still more than 20 dB lower than the path loss assumed here.
- *PLF2:* This is the second of two models in [3] and given by

$$PL(d) = 61.4 + 32 \log_{10}(d), \ d \text{ in meters.} \quad (2)$$

  This model is also consistently more than 20 dB lower than our model.
- *3GPP UMi:* The standard 3GPP urban micro (UMi) model with hexagonal deployments [35] is given by

$$PL(d) = 22.7 + 36.7 \log_{10}(d) + 26 \log_{10}(f_c), \quad (3)$$

  where d is distance in meters and f_c is the carrier frequency in GHz. It can be seen that, relative to the 3GPP UMi model at a conventional microwave frequency, f_c=2.5 GHz, the empirical 28 GHz model shows approximately 40 dB greater path loss.

We conclude that the mmW propagation model used here is significantly worse than path losses in current microwave frequencies as well as free space and other models used in earlier evaluation studies of mmW systems. As described above, this high path loss is a result of the NLOS propagation assumption implicit in the data on which the models are based. Nevertheless, we will see that with appropriate beamforming, mmW systems can still offer an order of magnitude improvement in capacity.

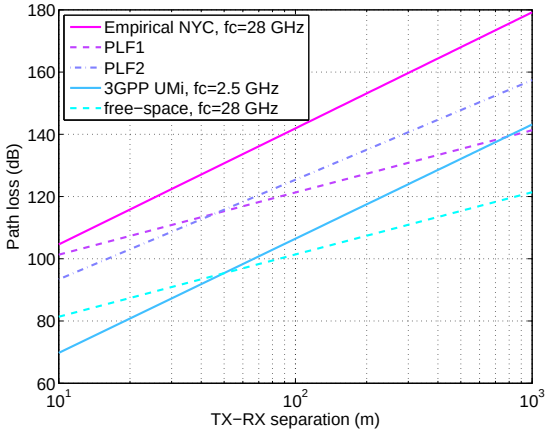

Fig. 2: Comparison of path loss models: (i) Empirical model based on NYC data [22], [24] used in this study; (ii) PLF1 and PLF2 models in the Samsung mmW study [3]; (iii) 3GPP Urban Micro path loss model [35] at $f_c = 2.5$ GHz; and (iv) Friis' law for free-space propagation at $f_c = 28$ GHz.

TABLE II: Default network parameters

Parameter	Description
BS layout and sectorization	Hexagonally arranged cell sites with three cells per site placed in a 2km x 2km square area.
UE layout	Uniformly dropped in area with average of 10 UEs per BS cell (i.e. 30 UEs per cell site).
Inter-site distance (ISD)	200 m
Carrier frequency	28 GHz
Duplex mode	TDD
Transmit power	20 dBm (uplink), 30 dBm (downlink)
Noise figure	5 dB (BS), 7 dB (UE)

III. System Modeling

A. Network Topology

We follow a standard cellular evaluation methodology [35] where the base stations (BSs) and user equipments (UEs) are randomly "dropped" according to some statistical model and the performance metrics are then measured over a number of random realizations of the network. Since we are interested in small cell networks, we follow a BS and UE distribution similar to the 3GPP Urban Micro (UMi) model in [35] with some parameters taken from the Samsung mmW study [3], [4]. The specific parameters are shown in Table II. Similar to 3GPP UMi model, the base station cell sites are distributed in a uniform hexagonal pattern with three cells (sectors) per site covering a 2 km by 2 km area with an inter-site distance (ISD) of 200 m. This layout leads to 130 cell sites (390 cells) per drop. UEs are uniformly distributed over the area at a density of 10 UEs per cell – which also matches the 3GPP UMi assumptions.

The maximum transmit power of 20 dBm at the UE and 30 dBm are taken from [3], [4]. These transmit powers are reasonable since current CMOS RF power amplifiers in the mmW range exhibit peak efficiencies of at least 8% [38], [39]. This implies that the UE TX power of 20 dBm and BS TX power of 30 dBm can be achieved with powers of 1.25W and 12.5W, respectively.

B. Beamforming Modeling

As described in the Introduction, an essential component of mmW systems is the ability to utilize very high-dimensional antenna arrays at the base station and mobile. In this work, we make the simplifying assumption that only single stream processing is considered and that beamforming is designed to maximize SNR without regard to interference. It is possible that more advanced techniques such as inter-cell coordinated beamforming and MIMO spatial multiplexing [32], [40] may offer further gains, particularly for mobiles close to the cell. Thus, the gains of mmW systems may be even higher, although as we will see below, under our NLOS propagation models, many mobiles are power-limited and the gains of spatial multiplexing may be limited.

Under the assumption of signal stream processing, the link between each TX-RX pair can be modeled as an effective single-input single-output (SISO) channel with an effective path loss that accounts for the total power received on the different path clusters between the TX and RX and the beamforming applied at both ends of the link. As shown in Appendix B, the effective SISO path loss (in dB) can be written as

$$PL = PL_{\rm omni} - \xi, \tag{4}$$

where $PL_{\rm omni}$ is the omni-directional path loss in (1) and ξ is a random variable accounting for the average beamforming gain.

We assume that mobiles are served by the base station cells with the lowest omni-directional path loss $PL_{\rm omni}$ – which can be determined by the UE monitoring the received power of appropriate synchronization signals broadcast from the base stations. Once the serving and interfering cells are identified for each UE, the beamforming gains ξ are then computed for all the serving links, assuming the beamforming directions are adjusted to maximize the beamforming gains along the serving links. After the beamforming weights are computed at all the transmitters, the average interference power can be computed by applying the same beamforming weights on the interfering links. In the downlink, where the BS will change the beamforming weights as it serves different users, we average the interference over the different users assuming equal time to each UE.

In a LOS channel, the beamforming gain will be as high as $N_t N_r$ where N_t and N_r are the number of TX and RX antennas. Since our simulations assume 64 antennas at both sides of the link, this LOS gain could be theoretically as high as 36 dB. However, the actual gain is somewhat lower since the power in the channel is spread over the $K = 3$ clusters with angular spread in each cluster (see Table I). In addition, since the coherence time of mmW systems can be very low, even with TDD operation, it may not be feasible to track the full channel matrix at either the TX or RX. Our approach is to assume that both the TX and RX on each link can, however, track the long-term second-order statistics which depend only on the large scale channel parameters (such as the per cluster path loss, shadowing, center angle of arrivals and angular spreads) but not the small-scale fading coefficients. This long-term beamforming model [41] reduces the gains somewhat further but provides a more realistic and conservative capacity estimate. Appendix B describes the beamforming assumptions in more detail.

C. SNR to Rate Mapping

Once the effective path losses are determined between all TX-RX pairs, we can compute the average SINR at each RX. The SINR in turn determines the rate per unit time and bandwidth allocated to the mobile. In an actual cellular system, the achieved rate (goodput) will depend on the average SNR through a number of factors including the channel code performance, channel quality indicator (CQI) reporting, rate adaptation and Hybrid automatic repeat request (HARQ) protocol. In this work, we abstract this process and assume a simplified, but widely-used, model [42], where the spectral efficiency is assumed to be given by the Shannon capacity with some loss Δ:

$$\rho = \min\left\{\log_2\left(1 + 10^{0.1(\mathsf{SNR}-\Delta)}\right), \rho_{max}\right\}, \tag{5}$$

where ρ is the spectral efficiency in bps/Hz, the SNR and loss factor Δ are in dB, and ρ_{max} is the maximum spectral efficiency. Based on analysis of current LTE turbo codes, the paper [42] suggests parameters $\Delta = 1.6$ dB and $\rho_{max} = 4.8$ bps/Hz. Assuming similar codes can be used for a mmW system, we apply the same ρ_{max} in this simulation, but increase Δ to 3 dB to account for fading. Note that all rates stated in this paper *do not* include the half duplex loss, which must be added depending on the UL-DL ratio. The one exception to this accounting is the comparison in Section IV-A between mmW and LTE systems, where we explicitly assume a 50-50 UL-DL duty cycle.

D. Downlink Scheduling

We use proportional fair scheduling with full buffer traffic. Since we assume that we cannot exploit multi-user diversity and only schedule on the average channel conditions, the proportional fair assumption implies that each UE will get an equal fraction of the time-frequency resources.

E. Uplink Scheduling

In uplink, we also assume full buffer traffic with proportional fair scheduling. In contrast with the downlink, in the uplink different multiple access schemes result in different capacities. If BS allows one UE to transmit for a portion of time in the whole band, the total transmit power will be limited to the transmit power of one user. If all UEs are allowed to transmit all time but on different subbands, then the total transmit power will be multiplied by the number of UEs

in the environment, which is advantageous for power limited systems. Therefore, we assume FDMA is performed in uplink unless otherwise stated.

As we shall show later in Fig. 6, for most mobiles, receiver thermal noise is the dominant factor, rather than interference. Hence, we currently do not perform any uplink power control and assume all UEs transmit at the maximum power. Nevertheless, incorporating power control will offer some further gains and will be useful future work.

IV. Results and Discussion

A. Uplink and Downlink Capacity

We plot SINR and rate distributions in Fig. 3 and Fig. 4 respectively. The downlink and uplink have similar distributions even though downlink TX power is 10 dB higher than the uplink. This is due to the fact that the uplink uses FDMA, where 10 UEs transmit simultaneously amounting to a 10-fold increase in total transmit power.

Also, although the SINR distribution for cellular networks in traditional frequencies is not plotted here, distributions found in cellular evaluation studies [35] appear to match reasonably closely with the downlink SINR cumulative distribution function (CDF) in the mmW range in Fig. 3, provided the TX power is sufficiently high. For example, at a BS TX power of 30 dBm, only about 20% of the mobiles appear under 0 dB, with virtually all mobiles greater than -10 dBm – which is very similar to conventional cellular SINR CDFs.

Table III provides a comparison of mmW and current LTE systems. The LTE capacity numbers are taken from the average of industry reported evaluations given in [35] – specifically Table 10.1.1.1-1 for the downlink and Table 1.1.1.3-1 for the uplink. The LTE evaluations include advanced techniques such as SDMA, although not coordinated multipoint. For the mmW capacity, we assumed 50-50 UL-DL TDD split and a 20% control overhead in both the UL and DL directions.

Under these assumptions, we see that the mmW system provides a significant 15-fold increase of overall cell capacity over the LTE system. Of course, most of the gains are simply coming from the increased spectrum: the operating bandwidth of mmW is chosen as 1 GHz as opposed to 20+20 MHz in LTE – so the mmW system has 25 times more bandwidth. Moreover, this is a basic mmW system with no spatial multiplexing or other advanced techniques – we expect even higher gains when advanced technologies are applied to optimize the mmW system.

However, the 5% cell edge rates are less dramatic and only offer a 5 fold increase. This indicates a significant limitation of mmW systems under NLOS propagation – edge of cell users become power-limited and are unable to exploit the increased spectrum. Thus, other features will be needed achieve a more uniform performance in mmW systems in these scenarios.

B. Interference vs. Power-Limited Regime

The empirical CDFs of the downlink/uplink rate per UE are shown in Fig. 5. It is observed that although rate distribution generally improves as bandwidth increases, the marginal gain diminishes as bandwidth approaches 1 GHz. This implies that

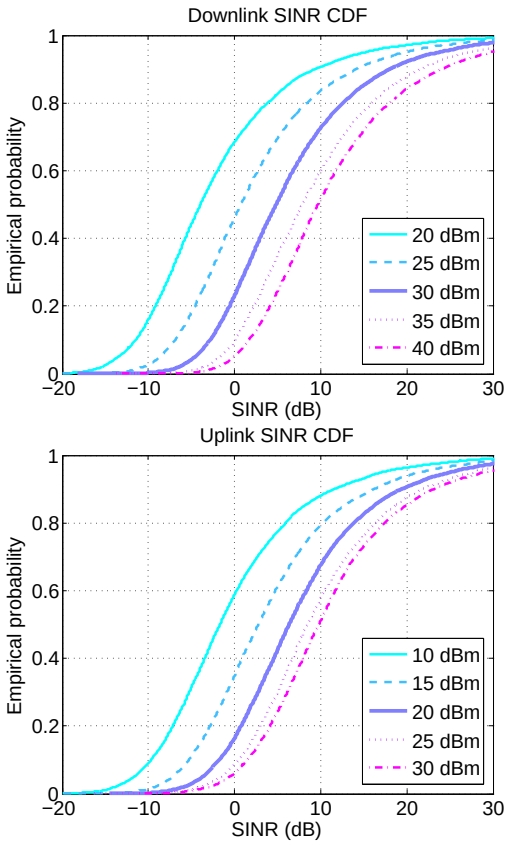

Fig. 3: Downlink (top plot) / uplink (bottom plot) SINR CDF with varying TX power

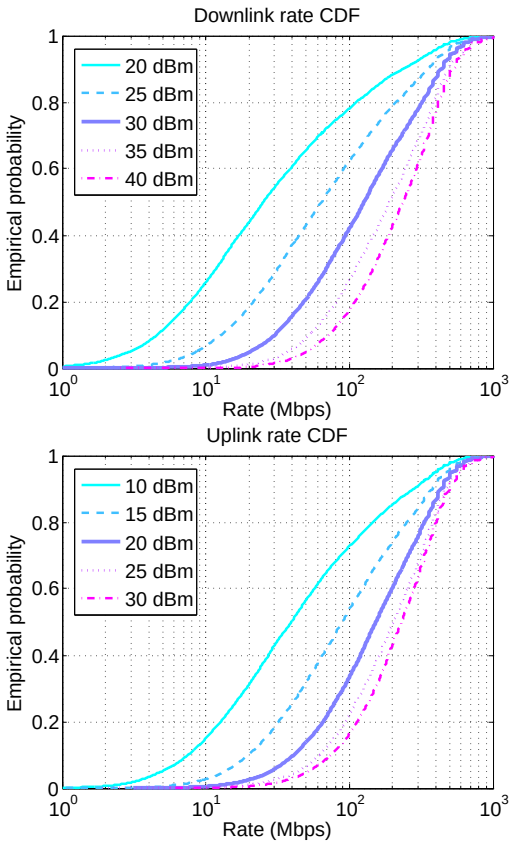

Fig. 4: Downlink (top plot) / uplink (bottom plot) rate CDF with varying TX power

TABLE III: mmW and LTE cell capacity/cell edge rate comparison, assuming 20% overhead and 50% UL-DL duty cycle for the mmW system.

System antenna	BW & Duplex	fc (GHz)	Cell capacity (Mbps)	Cell edge rate (Mbps, 5%)
mmW 64x64	1 GHz TDD	28	780 (DL) 850 (UL)	8.22 (DL) 11.3 (UL)
LTE 2x2 DL, 2x4 UL	20+20 MHz FDD	2.5	53.8 (DL) 47.2 (UL)	1.80 (DL) 1.94 (UL)

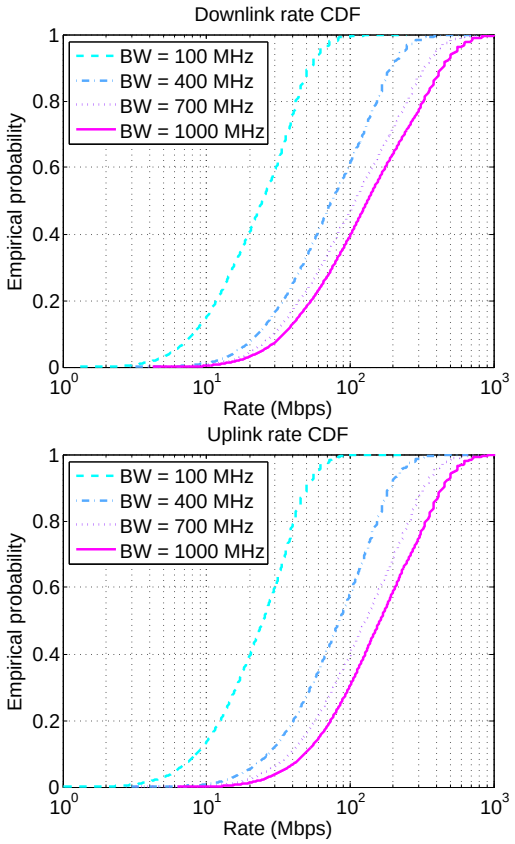

Fig. 5: Downlink (top plot) / uplink (bottom plot) rate CDF with varying bandwidth

a mmW system with multi-GHz bandwidth may be power-limited and the degrees of freedom in the bandwidth are likely to be under-utilized if NLOS propagation is dominant. As a result, multiple antennas should be operated in the beamforming mode to reduce signal attenuation due to path loss, rather than the spatial multiplexing mode, which benefits only in the high power regime.

As further evidence that mmW systems are power-limited, the empirical CDFs of interference to noise ratio (INR) given in Fig. 6 show that the noise power is dominant more often both in uplink and downlink. Consequently, interference management technologies such as power control, coordinated beamforming, and interference cancellation will have less impact in the mmW frequencies than they do in current cellular systems, if NLOS propagation is dominant. On the other hand, multihop relaying, as a method of reducing effective TX-RX

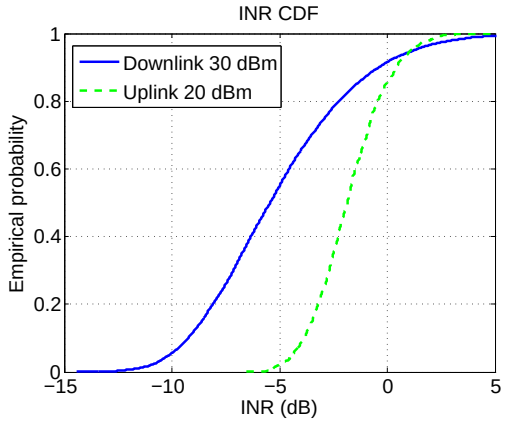

Fig. 6: Downlink/uplink interference to noise ratio distribution

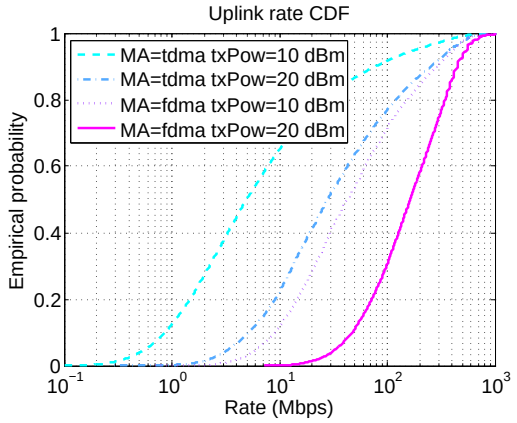

Fig. 7: Uplink rate CDF vs multi-access schemes

distance, may play a much more important role in mmW, since the bottleneck is no longer the degrees of freedom, but rather the raw received power, a scenario that is the exact opposite of the current interference-limited cellular systems.

C. Implications for Device Requirements and Multiple Access

As pointed out in prior work [3], [4], the cost of implementing analog-to-digital converter (ADC) and digital-to-analog converter (DAC) that are capable of supporting multi-Gbps transmission could be prohibitive for a mmW system with large antenna arrays. Hence, it may be favorable to choose RF or IF beamforming (one ADC/DAC per RF chain, beamform to one direction at a time) over digital beamforming (one ADC/DAC per antenna, beamform to multiple directions simultaneously) by forgoing the support of multi-stream and multi-user transmissions. However, according to the uplink rate CDF shown in Fig. 7, one can easily see an order of magnitude improvement when multi-user transmission is enabled by FDMA, compared to a baseline TDMA. Despite the high cost, there is still very good motivation to pursue multi-user support and advance technologies aiming at reducing complexity/cost of ADC/DAC [43] that will likely to play a vital role in a practical multi-Gbps mmW system deployment.

CONCLUSIONS

In this paper we have provided system level simulations to evaluate the capacity of mmW cellular systems using channel models based on urban experimental path loss data. Our results have shown that, even under a conservative model where all users experience NLOS propagation, mmW systems can provide a 15-fold improvement in data rates compared with the current LTE systems. Under this model, the mmW system becomes power limited rather than interference limited, necessitating different design methodologies than the current LTE systems. As a future research, power efficient beamforming at different subbands can be studied in order to utilize FDMA in the uplink and multihop relaying in downlink can be included to simulations to exploit the unused degrees of freedom and to extend the range. Another future step can be the reevaluation of mmW system which contain both LOS and NLOS connections.

ACKNOWLEDGEMENTS

The authors would like to deeply thank Prof. Rappaport's research group for providing the path loss models [22]–[25] that made this research possible: Yaniv Azar, Felix Gutierrez, DuckDong Hwang, Rimma Mayzus, George McCartney, Shuai Nie, Mathew Samimi, Jocelyn K. Schulz, Shu Sun, Kevin Wang, George N. Wong and Hang Zhao. This work also benefitted significantly from discussions with our industrial partner InterDigital, particularly Doug Castor, Tao Deng, Robert DiFazio, Phil Pietraski and Ravi Pragada.

APPENDIX A
SMALL SCALE MIMO MODEL

As described in Section II, the link between each BS and UE is specified by a set of large-scale parameters including the number of path clusters and the per cluster path losses, center angles and angular spreads. These large-scale parameters are assumed to be constant. However, small-scale fading will result in variations of the channel in time and frequency. To capture the effects of small-scale fading, we follow a standard model [35], [36], where the complex baseband MIMO channel matrix $\mathbf{H}$ at each time and frequency is modeled as a random matrix of the form

$$\mathbf{H} = \sum_{\ell=1}^{L} g_\ell \mathbf{e}_R(\theta_\ell^R, \phi_\ell^R)\mathbf{e}_T^*(\theta_\ell^T, \phi_\ell^T), \tag{6}$$

where L is the number of subpaths, and for each subpath ℓ, g_ℓ is a random small-scale fading coefficient, and $(\theta_\ell^T, \phi_\ell^T)$ and $(\theta_\ell^R, \phi_\ell^R)$ are respectively the azimuth and elevation AoD and AoA of the subpath. The vectors $\mathbf{e}_T(\theta,\phi)$ and $\mathbf{e}_R(\theta,\phi)$ are the complex unit vector spatial responses of the antenna to a path at angles (θ,ϕ). As shown in Table I, we assume that $\mathbf{e}_T(\theta,\phi)$ and $\mathbf{e}_R(\theta,\phi)$ are the response vectors for a 2D linear array with $\lambda/2$-frequency spacing.

To describe the distribution on the subpath parameters, we assume that each subpath ℓ randomly belongs to one of the K clusters with equal probabilities. We let $\eta_\ell \in \{1,\ldots,K\}$ be the random cluster index for the ℓ-th path. Conditional on $\eta_\ell = k$, we assume that the parameters $(g_\ell, \theta_\ell^R, \theta_\ell^T)$ are distributed as:

$$\begin{aligned} g_\ell &\sim \mathcal{C}N(0, G_k), \\ \theta_\ell^R &\sim \overline{\theta}_k^R + U[-\delta_k^R, \delta_k^R], \quad \theta_\ell^T \sim \overline{\theta}_k^T + U[-\delta_k^T, \delta_k^T] \end{aligned}$$

where $\overline{\theta}_k^R, \overline{\theta}_k^T$ are the cluster azimuthal TX and RX central angles, δ_k^R, δ_k^T are the TX and RX cluster angular spreads and G_k is the cluster average channel gain in linear scale

$$G_k = \frac{K}{L} 10^{-0.1\mathrm{PL}_k}, \tag{7}$$

where PL_k is the path loss of the k-th cluster. We assume that the subpath parameters $(\eta_\ell, g_\ell, \theta_\ell^R, \theta_\ell^T)$ are independent for different subpaths ℓ. Also, since we assume no vertical angular spread, the vertical angles are given by

$$\phi_\ell^R = \overline{\phi}^R, \quad \phi_\ell^T = \overline{\phi}^T$$

for all subpaths ℓ. In all our simulations, we take L to be a large value $L = 100$.

APPENDIX B
ESTIMATION OF THE BEAMFORMING GAIN

Since beamforming is an essential component in mmW systems, it is worthwhile to briefly discuss how the beamforming is precisely modeled in this study: If the MIMO channel matrix between some TX-RX pair is $\mathbf{H}$ and the transmitter and receiver apply beamforming vectors $\mathbf{u}_T$ and $\mathbf{u}_R$, the channel will appear as a SISO channel with an instantaneous gain $\mathbf{u}_R^*\mathbf{H}\mathbf{u}_T$. Now, in the model (6), the small-scale channel coefficients g_ℓ are assumed to be complex normal with zero mean. It follows that for any fixed set of large-scale parameters and beamforming vectors, the channel will be a Rayleigh fading SISO channel with average gain,

$$G_{\mathrm{BF}} = G_{\mathrm{BF}}(\mathbf{u}_T, \mathbf{u}_R) := \mathbb{E}\left|\mathbf{u}_R^*\mathbf{H}\mathbf{u}_T\right|^2,$$

where the expectation is taken holding all the large-scale parameters constant and averaging over the small scale parameters.

We will let G_{omni} denote the *omni-directional* gain, meaning the value $G_{\mathrm{BF}}(\mathbf{u}_T, \mathbf{u}_R)$ averaged uniformly over all all unit beamforming vectors $\mathbf{u}_R$ and $\mathbf{u}_T$:

$$G_{\mathrm{omni}} = \int_{\|\mathbf{u}_T\|=\|\mathbf{u}_R\|=1} G_{\mathrm{BF}}(\mathbf{u}_T, \mathbf{u}_R) d\mathbf{u}_R d\mathbf{u}_T.$$

It is easy to check that from the model (6) and the normalization assumption (7),

$$G_{\mathrm{omni}} = \mathbb{E}\|\mathbf{H}\|_F^2 = \sum_{k=1}^{K} 10^{-0.1PL_k}.$$

We define the *omni-directional path loss* as the inverse of the omni-directional gain (in dB)

$$\begin{aligned} PL_{\mathrm{omni}} &:= -10\log_{10} G_{\mathrm{omni}} \\ &= -10\log_{10}\left[\sum_{k=1}^{K} 10^{-0.1PL_k}\right]. \end{aligned} \tag{8}$$

This omni-directional path loss represents the average path loss when the beamforming weights are placed in random directions. Obviously, proper selection of the beamforming weights can reduce the path loss significantly.

There are two methods to perform beamforming: instantaneous and long-term. Instantaneous (or short-term) beamforming corresponds to the case when the beamforming weight vectors can be adapted to the instantaneous channel matrix $\mathbf{H}$. Instantaneous beamforming would result in an average channel gain of

$$\mathbb{E}\left[\max_{\|\mathbf{u}_R\|=\|\mathbf{u}_T\|=1} |\mathbf{u}_R^* \mathbf{H} \mathbf{u}_T|^2\right].$$

However, obtaining this instantaneous beamforming gain may be impractical, even in TDD, since it requires tracking a large number of channel matrix parameters. Such tracking may be particularly difficult in a mmW system where the coherence time may be small due to the high carrier frequency.

In this paper, we therefore take a conservative approach and assume we can only apply *long-term* beamforming as described in [41]. In long-term beamforming, the TX and RX are assumed to adapt the beamforming vectors to the large-scale parameters (which are relatively slowly varying) but not the small-scale ones. Under this assumption, the optimal beamforming vectors are given by

$$\begin{aligned}(\widehat{\mathbf{u}}_T, \widehat{\mathbf{u}}_R) &= \arg\max_{\|\mathbf{u}_R\|=\|\mathbf{u}_T\|=1} G_{\mathrm{BF}}(\mathbf{u}_T, \mathbf{u}_R) \\ &= \arg\max_{\|\mathbf{u}_R\|=\|\mathbf{u}_T\|=1} \mathbb{E}\left|\mathbf{u}_R^* \mathbf{H} \mathbf{u}_T\right|^2, \end{aligned} \quad (9)$$

where the maximization is outside the expectation to model the fact that the beamforming weights are not adapted to the small-scale fading. Recall that, in the expectation, we are holding the large-scale fading parameters constant.

The optimization (9) is non-convex and cannot, in general, be solved optimally jointly over $\mathbf{u}_T$ and $\mathbf{u}_R$. However, the individual optimization over $\mathbf{u}_T$ and $\mathbf{u}_R$ can be performed by finding a maximum eigenvector. Thus, we can approximately solve the optimization by alternately optimizing over $\mathbf{u}_T$ and $\mathbf{u}_R$ separately.

Now, given any beamforming vectors $\mathbf{u}_T$ and $\mathbf{u}_R$ we can define the *beamforming gain* as the difference (in dB) between the the gain with beamforming and the omni-directional gain:

$$\xi := 10\log_{10}\left[\frac{G_{\mathrm{BF}}(\mathbf{u}_T, \mathbf{u}_R)}{G_{\mathrm{omni}}}\right]$$

With a beamforming gain ξ, the effective path loss of the channel becomes

$$PL = PL_{\mathrm{omni}} - \xi,$$

so the beamforming gain can be interpreted as a reduction in the path loss.

Fig. 8 plots the cumulative distribution functions of the beamforming gains ξ on both the serving and interfering links. For the serving links, the beamforming vectors are selected to maximize the beamforming gain as in (9). When we apply these beamforming vectors on a second random matrix $\mathbf{H}$ generated with an independent set of large-scale parameters, we obtain the beamforming gain on the interfering links. Both the serving and interfering beamforming gains are random variables since they depend on the random large-scale parameters.

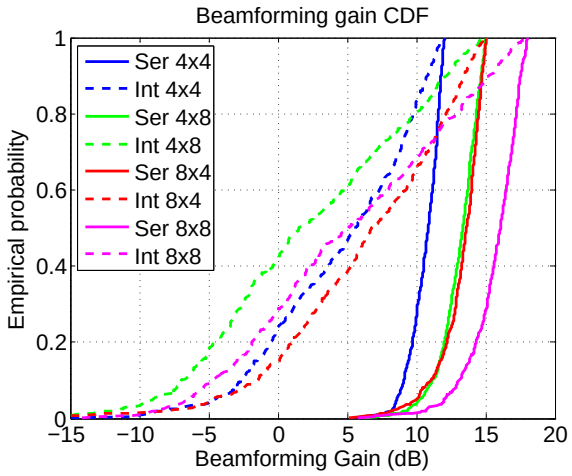

Fig. 8: Empirical CDF of the beamforming gain (azimuth-only) for serving (Ser) and interfering (Int) links with N_t and N_r antenna elements in the horizontal direction at the TX and RX, respectively.

The figure shows the azimuth-only gain for different numbers of antennas in the horizontal direction. Since our model assumes no vertical angular separation or vertical angular spread (see Table I), we will obtain the full vertical gains for all links (interfering and serving). Thus, if the TX has a 2D array with $N_t \times N_t$ elements, and the RX has a 2D array with $N_r \times N_r$ elements, the resulting total beamforming gain (in dB) will be the sum of azimuthal gain from Fig. 8 and $10\log_{10}(N_t N_r)$. We see from Fig. 8 that, even with the long-term beamforming and angular spread over three clusters, we often obtain an average beamforming gain 2-3 dB from the maximum and often more than 10 dB separation from the interferers.

REFERENCES

[1] Cisco, "Cisco Visual Network Index: Global mobile traffic forecast update," 2012.

[2] "2020: Beyond 4G: Radio evolution for the gigabit experience," Nokia Siemens Networks, white paper, 2011, available online at http://www.nokiasiemensnetworks.com/file/15036/2020-beyond-4g-radio-evolution-for-the-gigabit-experience.

[3] F. Khan and Z. Pi, "Millimeter-wave Mobile Broadband (MMB): Unleashing 3-300GHz Spectrum," in *Proc. IEEE Sarnoff Symposium*, Mar. 2011.

[4] ——, "An introduction to millimeter-wave mobile broadband systems," *IEEE Comm. Mag.*, vol. 49, no. 6, pp. 101 – 107, Jun. 2011.

[5] T. Rappaport, J. Murdock, and F. Gutierrez, "State of the art in 60-GHz integrated circuits and systems for wireless communications," *Proceedings of the IEEE*, vol. 99, no. 8, pp. 1390 – 1436, August 2011.

[6] P. Pietraski, D. Britz, A. Roy, R. Pragada, and G. Charlton, "Millimeter wave and terahertz communications: Feasibility and challenges," *ZTE Communications*, vol. 10, no. 4, pp. 3–12, Dec. 2012.

[7] C. Doan, S. Emami, D. Sobel, A. Niknejad, and R. Brodersen, "Design considerations for 60 GHz CMOS radios," *IEEE Comm. Mag.*, vol. 42, no. 12, pp. 132 – 140, 2004.

[8] C. Doan, S. Emami, A. Niknejad, and R. Brodersen, "Millimeter-wave CMOS design," *IEEE J. Solid-State Circuts*, vol. 40, no. 1, pp. 144–155, 2005.

[9] Y.-P. Zhang and D. Liu, "Antenna-on-Chip and Antenna-in-Package solutions to highly integrated millimeter-wave devices for wireless communications," *IEEE Trans. Antennas and Propagation*, vol. 57, no. 10, pp. 2830–2841, 2009.

[10] J. Nsenga, A. Bourdoux, and F. Horlin, "Mixed analog/digital beamforming for 60 GHz MIMO frequency selective channels," in *Proc. ICC*, 2010.

[11] S. Rajagopal, S. Abu-Surra, Z. Pi, and F. Khan, "Antenna array design for multi-gbps mmwave mobile broadband communication," in *Proc. Globecomm*, 2011.

[12] K.-C. Huang and D. J. Edwards, *Millimetre Wave Antennas for Gigabit Wireless Communications: A Practical Guide to Design and Analysis in a System Context*. Wiley Publishing, 2008.

[13] F. Rusek, D. Persson, B. K. Lau, E. Larsson, T. Marzetta, O. Edfors, and F. Tufvesson, "Scaling up MIMO: Opportunities and challenges with very large arrays," *IEEE Signal Process. Mag.*, vol. 30, no. 1, pp. 40–60, 2013.

[14] E. Perahia, C. Cordeiro, M. Park, and L. Yang, "IEEE 802.11ad: Defining the next generation multi-Gbps Wi-Fi," in *Proc. IEEE Cons. Comm. & Network. Conf.*, Jan. 2010.

[15] S. J. Vaughan-Nichols, "Gigabit Wi-Fi is on its way," *IEEE Computer*, Nov. 2010.

[16] T. Baykas, C.-S. Sum, Z. Lan, J. Wang, M. A. Rahman, H. Harada, and S. Kato, "IEEE 802.15.3c: The first IEEE wireless standard for data rates over 1 Gb/s," *IEEE Comm. Mag.*, Jul. 2011.

[17] T. S. Rappaport, *Wireless Communications: Principles and Practice*, 2nd ed. Upper Saddle River, NJ: Prentice Hall, 2002.

[18] K. Allen *et al.*, *Building penetration loss measurements at 900 MHz, 11.4 GHz, and 28.8 MHz*, ser. NTIA report – 94-306. Boulder, CO: U.S. Dept. of Commerce, National Telecommunications and Information Administration, 1994.

[19] C. Anderson and T. Rappaport, "In-building wideband and partition loss measurements at 2.5 and 60 GHz," *IEEE Trans. Wireless Comm.*, vol. 3, no. 3, pp. 922 – 928, May 2004.

[20] A. Alejos, M. Sanchez, and I. Cuinas, "Measurement and analysis of propagation mechanisms at 40 GHz: Viability of site shielding forced by obstacles," *IEEE Trans. Vehicular Technology*, vol. 57, no. 6, pp. 3369–3380, 2008.

[21] J. S. Lu, D. Steinbach, P. Cabrol, and P. Pietraski, "Modeling human blockers in millimeter wave radio links," *ZTE Communications*, vol. 10, no. 4, pp. 23–28, Dec. 2012.

[22] Y. Azar, G. N. Wong, K. Wang, R. Mayzus, J. K. Schulz, H. Zhao, F. Gutierrez, D. Hwang, and T. S. Rappaport, "28 GHz propagation measurements for outdoor cellular communications using steerable beam antennas in New York City," in *Proc. ICC (to appear)*, 2013.

[23] H. Zhao, R. Mayzus, S. Sun, M. Samimi, J. K. Schulz, Y. Azar, K. Wang, G. N. Wong, F. Gutierrez, and T. S. Rappaport, "28 GHz millimeter wave cellular communication measurements for reflection and penetration loss in and around buildings in New York City," in *Proc. ICC (to appear)*, 2013.

[24] M. Samimi, K. Wang, Y. Azar, G. N. Wong, R. Mayzus, H. Zhao, J. K. Schulz, S. Sun, F. Gutierrez, and T. S. Rappaport, "28 GHz angle of arrival and angle of departure analysis for outdoor cellular communications using steerable beam antennas in New York City," in *Proc. IEEE VTC (to appear)*, 2013.

[25] ——, "28 GHz path loss models in New York City," in *Proc. Globecomm (submitted)*, 2013.

[26] T. Zwick, T. Beukema, and H. Nam, "Wideband channel sounder with measurements and model for the 60 GHz indoor radio channel," *IEEE Trans. Vehicular Technology*, vol. 54, no. 4, pp. 1266 – 1277, July 2005.

[27] F. Giannetti, M. Luise, and R. Reggiannini, "Mobile and personal communications in 60 GHz band: A survey," *Wirelesss Personal Comunications*, vol. 10, pp. 207 – 243, 1999.

[28] C. Anderson and T. Rappaport, "In-building wideband partition loss measurements at 2.5 and 60 GHz," *IEEE Wireless Comm.*, vol. 3, no. 3, pp. 922 – 928, May 2004.

[29] P. Smulders and A. Wagemans, "Wideband indoor radio propagation measurements at 58 GHz," *Electronics Letters*, vol. 28, no. 13, pp. 1270 –1272, June 1992.

[30] T. Manabe, Y. Miura, and T. Ihara, "Effects of antenna directivity and polarization on indoor multipath propagation characteristics at 60 GHz," *IEEE J. Sel. Areas Comm.*, vol. 14, no. 3, pp. 441 –448, April 1996.

[31] H. Xu, V. Kukshya, and T. Rappaport, "Spatial and temporal characteristics of 60 GHz indoor channel," *IEEE J. Sel. Areas Comm.*, vol. 20, no. 3, pp. 620 – 630, April 2002.

[32] H. Zhang, S. Venkateswaran, and U. Madhow, "Channel modeling and MIMO capacity for outdoor millimeter wave links," in *Wireless Communications and Networking Conference (WCNC)*, April 2010.

[33] E. Torkildson, H. Zhang, and U. Madhow, "Channel modeling for millimeter wave MIMO," in *Proc. Information Theory and Applications Workshop (ITA)*, Feb. 5 2010.

[34] H. Zhang and U. Madhow, "Statistical modeling of fading and diversity for outdoor 60 GHz channels," in *International Workshop on mmWave Communications: from Circuits to Networks (mmCom10)*, September 2010.

[35] 3GPP, "Further advancements for E-UTRA physical layer aspects," TR 36.814 (release 9), 2010.

[36] ITU, "M.2134: Requirements related to technical performance for IMT-Advanced radio interfaces," Technical Report, 2009.

[37] S. Akoum, O. E. Ayach, and R. W. Heath, "Coverage and capacity in mmWave MIMO systems," in *Proc. of Asilomar Conf. on Signals, Syst. & Computers*, Pacific Grove, CA, Nov. 2012.

[38] S. Pinel *et al.*, "A 90nm CMOS 60GHz Radio," in *Proc. IEEE International Solid-State Circuits Conference.* , 2008.

[39] C. Marcu *et al.*, "A 90 nm CMOS Low-Power 60 GHz Transceiver With Integrated Baseband Circuitry," *IEEE J. Solid-State Circuts*, vol. 44, pp. 3434–3447, 2009.

[40] A. Alkhateeb, O. E. Ayach, G. Leus, and J. Robert W. Heath, "Hybrid analog-digital beamforming design for millimeter wave cellular systems with partial channel knowledge," in *Proc. Information Theory and Applications Workshop (ITA)*, Feb. 2013.

[41] A. Lozano, "Long-term transmit beamforming for wireless multicasting," in *Proc. ICASSP*, vol. 3, 2007, pp. III–417–III–420.

[42] P. Mogensen, W. Na, I. Z. Kovács, F. Frederiksen, A. Pokhariyal, K. I. Pedersen, T. Kolding, K. Hugl, and M. Kuusela, "LTE capacity compared to the Shannon bound," in *Proc. IEEE VTC*, 2007.

[43] H. Zhang, S. Venkateswaran, and U. Madhow, "Analog multitone with interference suppression: Relieving the ADC bottleneck for wideband 60 ghz systems," in *Proc. Globecomm*, Nov. 2012.